Preprints (www.preprints.org) | NOT PEER-REVIEWED | Posted: 15 May 2017 doi:10.20944/preprints201705.0111.v1

Peer-reviewed version available at *Appl. Sci.* **2017**, *7*, 644; doi:10.3390/app7070644

Review

Lévy Statistics and Glassy Behavior of Light in Random Fiber Lasers

Cid B. de Araújo [1,*], Anderson S. L. Gomes [2] and Ernesto P. Raposo [3]

[1] Departamento de Física, Universidade Federal de Pernambuco, Recife – PE, 50670-901, Brazil; cid@df.ufpe.br
[2] Departamento de Física, Universidade Federal de Pernambuco, Recife – PE, 50670-901, Brazil; anderson@df.ufpe.br
[3] Laboratório de Física Teórica e Computacional, Departamento de Física, Universidade Federal de Pernambuco, Recife – PE, 50670-901, Brazil; ernesto@df.ufpe.br
* Correspondence: cid@df.ufpe.br; Tel.: +55-81-2126-7630

Abstract: The interest in random fiber lasers (RFLs), first demonstrated one decade ago, is still growing and their basic characteristics have been studied by several authors. RFLs are open systems that present instabilities in the intensity fluctuations due to the energy exchange among their non-orthogonal quasi-modes. In this work, we present a review of the recent investigations on the output characteristics of a continuous-wave erbium-doped RFL, with emphasis on the statistical behavior of the emitted intensity fluctuations. A progression from the Gaussian to Lévy and back to the Gaussian statistical regime was observed by increasing the excitation laser power from below to above the RFL threshold. By analyzing the RFL output intensity fluctuations, the probability density function of emission intensities was determined, and its correspondence with the experimental results was identified, enabling a clear demonstration of the analogy between the RFL phenomenon and the spin-glass phase transition. A replica-symmetry-breaking phase above the RFL threshold was characterized and the glassy behavior of the emitted light was established. We also discuss perspectives for future investigations on RFL systems.

Keywords: random fiber laser; Lévy statistics; photonic spin-glass behavior

1. Introduction

Proposals for operation of random lasers (RLs) were made five decades ago by Ambartsumyan and co-workers [1,2], who visualized the possibility of new kind of laser that does not require the use of optical cavities. Initially, they reported on the operation of a laser in which one of the cavity mirrors was replaced by a piece of paper that scattered the light in such way that a fraction of the backscattered light was enough to provide feedback for the laser operation. Following the original work, the same group published a series of papers studying the line-narrowing [3], frequency stability [4], and the statistical emission properties [5] of lasers with the so-called nonresonant feedback.

Apparently, the initial motivation for these studies was the observation of laser emission from interstellar media [6], and the interest of the group on this subject still continued in the subsequent years [7-9].

For about fifteen years the majority of the research on this theme was pursued by groups that concentrate their effort on the operation of RLs based on microcrystals doped by rare-earth ions [10]. However, the first efficient RL system built in a laboratory environment was reported in 1994 by Lawandy and co-workers [11], who demonstrated the operation of a RL based on dye molecules

© 2017 by the author(s). Distributed under a Creative Commons CC BY license.

Preprints (www.preprints.org) | NOT PEER-REVIEWED | Posted: 15 May 2017 doi:10.20944/preprints201705.0111.v1

Peer-reviewed version available at Appl. Sci. 2017, 7, 644; doi:10.3390/app7070644

dissolved in alcohol with suspended titanium dioxide particles. That report was followed by a great number of papers from different authors that investigated on other physical systems for efficient RL operation. A large variety of materials has been tested in the past years, and recent publications on RLs describe, for example, experiments with dyes dissolved in transparent liquids, gels or liquid crystals with suspended micro or nanoparticles as light scatterers [12-17], powders of semiconductor quantum dots [18,19], dielectric nanocrystals doped with rare-earth ions [20,21], polymers and organic membranes doped by luminescent molecules [22-27], semiconductor and metallic nanowires structures [28-31], and even atomic vapors that present analogies with astrophysical lasers [32].

There is a large literature on RLs motivated by the interest in a deeper understanding of the fundamental properties of RLs [33-36], as well as reports on their possible application in sensing [37], optofluidics [38,39], and imaging [40], among other fields [41]. Moreover, although from the fundamental point of view there are many reports focusing on the basic characteristics of RLs and their operation, the analogies between RLs and other complex systems have been investigated by experiments only recently. For example, in the work by Ghofraniha and co-authors [42], it was demonstrated for the first time the analogy between RLs and the spin-glass phenomenon.

In the present work, we review recent advances on the characteristics of random fiber lasers, which have great potential for applications in various areas, as mentioned below. In section 2, we describe the Materials and Methods used. In Section 3, the experiments with erbium-doped fibers to characterize the RL behavior and the analysis of the intensity fluctuations are presented, along with the theoretical framework to understand the system behavior. Finally, in section 4 a summary of the article contents and a discussion on perspectives for future work are presented.

2. Materials and Methods

2.1. Random Fiber Lasers

Random fiber lasers (RFLs) are akin to RLs, being the one-dimensional (1D) or quasi-1D version of the 2D or 3D RLs. They bear the same nonconventional remarkable characteristic: the optical feedback is provided by a scattering medium, rather than by fixed mirrors or fiber Bragg gratings (FBGs), as in conventional fiber lasers. Similarly to conventional fiber lasers, a gain medium is excited by an appropriate optical pump source. The first demonstrated RFL, by de Mattos and co-workers in 2007 [43], can be seen as a quasi-1D extension of the colloidal based RL reported by Lawandy and co-workers in 1994 [11]. In [43], the hollow core of a photonic crystal fiber was filled with a colloidal suspension of 250 nm rutile (TiO_2) particles in a rhodamine 6G solution. By transversely pumping with nanosecond pulses from the second harmonic of a Nd:YAG laser, directional emission was generated axially, and the feedback was due to the TiO_2 scatterers. Shortly after the report of ref. [43], Lizárraga and co-authors [44] and Gagné and Kashyap [45] demonstrated the operation of a continuous-wave (cw) pumped erbium-based RFL (Er-RFL) with random FBGs providing the scattering mechanism. We anticipate that this special type of RFL will be exploited as the photonic platform for all the work described here, and will be detailed later.

A new breakthrough in the research of RFLs occurred in 2010, when Turitsyn and co-workers [46] first reported the operation of a RFL exploiting the Rayleigh scattering as the optical feedback mechanism in long (~83 km) conventional single-mode optical fibers, whilst the gain mechanism was the stimulated Raman scattering excited in the fiber. After this work, the interest in RFLs and applications has fantastically grown, as reviewed in [47,48]. Indeed, by further exploiting the

Preprints (www.preprints.org) | NOT PEER-REVIEWED | Posted: 15 May 2017 doi:10.20944/preprints201705.0111.v1

Peer-reviewed version available at Appl. Sci. 2017, 7, 644; doi:10.3390/app7070644

Rayleigh mechanism due to refractive index fluctuations as the multiple light scattering mechanism, a myriad of novel types of RFLs have been demonstrated using stimulated Raman or Brillouin scattering process. As most of the works between 2007 and 2014 has been reviewed in [47,48], including polymer-based optical fibers or plasmonically-enhanced RFLs, we highlight here the diversity of works reported over the years 2015 and 2016 (see [49-66] and references therein). As examples, we mention that a Q-switched operation has been reported using Brillouin scattering [56], with pulses as short as 42 ns at 100 kHz being demonstrated. Regarding the fiber length, since the first observation of RFL made using conventional fibers with 83 km [46], RFLs with fiber lengths as short as 120 m has been reported [58], also providing 200 W of output power. Other recent features of RFLs include tunability using graphene based devices [56] or high-order Raman scattering [57], second harmonic generation [59], polarized emission from disordered polymer optical fiber [60], and photonic turbulence [67].

2.2 Fiber Bragg Grating Based Random Fiber Lasers

As mentioned above, FBG-based RFLs were first introduced in 2009 [44,45]. Currently, the FBG fabrication methods, characterization and management constitute a well-developed field, and further information on this subject is deferred to ref. [68]. Typically, a writing setup based, for instance, on cw UV radiation or femtosecond sources at 800 nm is employed to inscribe a FBG into a conventional or core-doped optical fiber. The case of interest here exploits an active core single-mode fiber, using Er^{3+} ions, which can be excited at 980 nm or 1480 nm, and emits in the 1540-1560 nm spectral region. Instead of inscribing the FBGs in an evenly spaced way, thus leading to conventional resonators, the erbium-based FBGs are randomly spaced and play the role of random scatterers, leading to RFL emission. Generally, the fiber is placed on a movable stage which is randomly displaced, thus providing the randomness in the FBG writing process. Several tens to hundreds of gratings can be inscribed along several tens of cm of fiber length. In the next section, we will describe the fabrication and characterization of the Er-RFL with a specially-designed FBG used [45] to study the Lévy-like statistics and observation of the replica-symmetry-breaking phenomenon, which marks the signature of the phase transition from a photonic paramagnetic to a photonic spin-glass phase.

3. Results

3.1 Characterization of the FBG-based Er-RFL Explored as a Statistical Physical Experimental Platform

As reported by Gagné and Kashyap [45], a unique FBG was produced by writing an exceptionally high number of gratings (>> 1000) over a 30 cm length fiber. A polarization-maintaining erbium-doped fiber from CorActive (peak absorption 28 dB/m at 1530 nm, NA 0.25, mode field diameter 5.7 μm) was employed, in which the randomly distributed phase errors grating was written, instead of a random array of gratings as in [44]. It was realized in [45] that during the movement of the translation stage, the friction between the fiber and the mount introduced irregularities in the grating spectrum that could be controlled by managing the air flow from the vacuum. Such irregularities were perceived as small phase errors, randomly but continuously distributed along the grating profile being inscribed. Thanks to this procedure, a very high number of modes was possible, which is very important for several applications, as we will see later. The Er-RFL described in [45] had a very low threshold of 3 mW, with a throughput efficiency

Preprints (www.preprints.org) | NOT PEER-REVIEWED | Posted: 15 May 2017 doi:10.20944/preprints201705.0111.v1

Peer-reviewed version available at Appl. Sci. 2017, 7, 644; doi:10.3390/app7070644

of ~4.5 % for 100 mW pump power. The number of emitted modes was dependent on the pump power and fiber length (20 or 30 cm fiber lengths were characterized in [45]), and a single or few modes were observed, limited by the system measurement resolution [69].

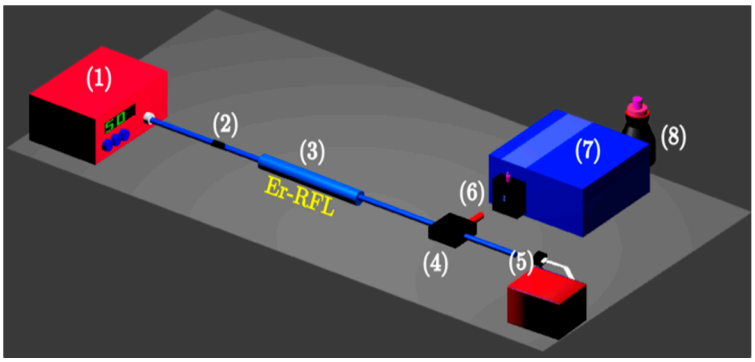

Figure 1. Experimental setup for the Er-RFL system. (1) Fiber pigtailed semiconductor laser. (2) Fiber connector. (3) Er-doped RFL. (4) WDM 1480-1550. (5) Power meter to measure the output power P_{out} at 1480 nm. (6) RFL emission out to the spectrometer. (7) Spectrometer. (8) Liquid-N_2 cooled InGaAs CCD camera. (Reproduced with permission from ref. [68].)

For the experiments described here, the 30 cm long fiber was employed with the experimental setup shown in Fig. 1, reproduced from ref. [68]. The pump source was a semiconductor laser operating in the cw regime at 1480 nm, delivering 150 mW output power at the fiber pigtail. The Er-RFL output was split, through a 1480 nm/1550 nm WDM, to a power meter and a spectrometer.

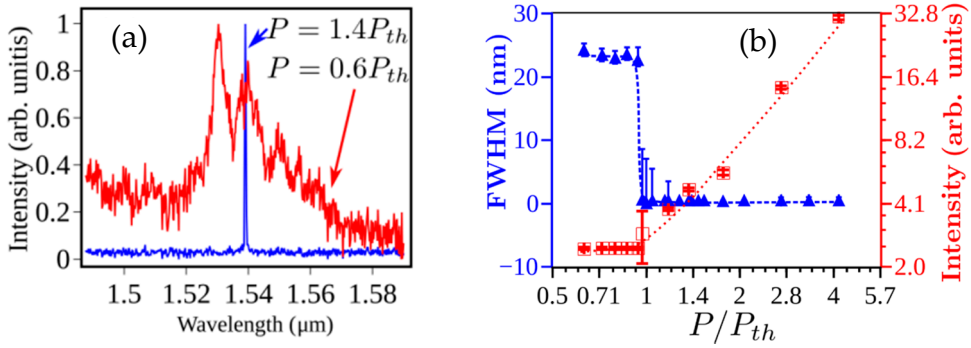

Figure 2. (a) Emitted spectrum of Er-RFL before (red) and after (blue) the laser threshold. **(b)** Emitted intensity (squares) and FWHM (triangles) of the Er-RFL system as a function of the normalized input power. The measured threshold power was P_{th} = 16.30 ± 0.05 mW. The dotted lines are guide to the eyes. (Reproduced with permission from ref. [68].)

Fig. 2(a) shows the Er-RFL output spectrum for intensities below and above the RFL threshold, while Fig. 2(b) shows the linewidth narrowing (left y-axis) and emitted Er-RFL intensity (right y-axis) as a function of pump power P normalized to the threshold power P_{th}. The threshold power was P_{th} = 16.30 ± 0.05 mW [68], which is higher than in the original work of ref. [45] due to the lossy components employed. However, this fact did not affect the experimental studies, and the output was typically around 1-2 mW.

Besides the routine characterization necessary for the statistical measurements illustrated in Fig. 2, two other important analyzes were performed in order to show that the laser is multimode, i.e, with many longitudinal modes, and that the intensity fluctuation does not depend on the pump laser fluctuation. To demonstrate the multimode characteristic of the Er-RFL, we employed [69] the

Preprints (www.preprints.org) | NOT PEER-REVIEWED | Posted: 15 May 2017 doi:10.20944/preprints201705.0111.v1

Peer-reviewed version available at Appl. Sci. 2017, 7, 644; doi:10.3390/app7070644

technique of speckle contrast, following the work of refs. [40,70,71]. To generate the speckle, a scattering medium with dried TiO_2 (250 nm) nanoparticles in water solution on a microscope slide along with a Kohler illumination system was used. Different CCD cameras were employed for the data acquisition, depending upon the source wavelength in the visible or in the near-infrared. The relation between the speckle contrast C and the number m of longitudinal modes of the source is given by [71] $C = \sigma/\langle I \rangle = 1/\sqrt{m}$, where σ and $\langle I \rangle$ are the standard deviation and the average intensity determined from the speckle, respectively. Figure 3 shows the obtained results for different light sources.

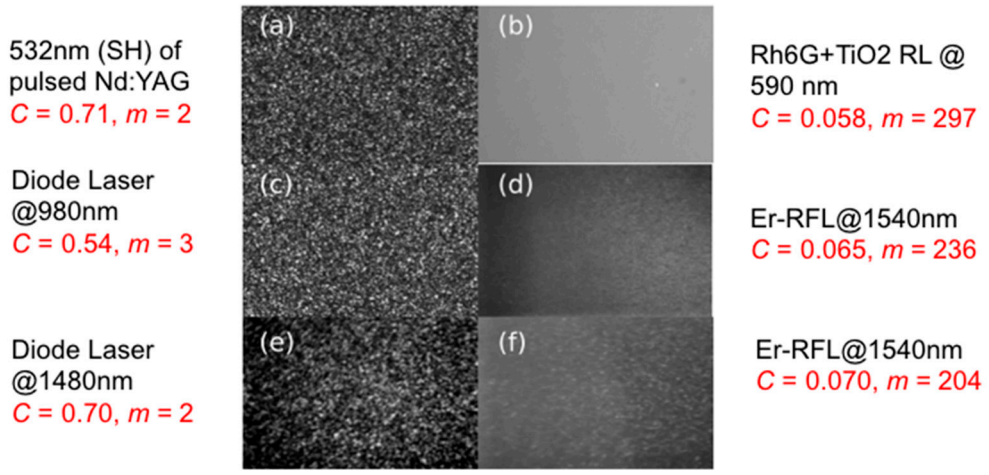

Figure 3. (a), **(c)** and **(e)** display the measured speckle of the second harmonic of a pulsed Nd:YAG laser **(a)**, a cw-diode laser operating at 980 nm **(c)**, and a similar diode laser but operating at 1480 nm **(e)**. **(b)**, **(d)** and **(f)** show a colloid RL **(b)**, the Er-RFL at 1540 nm pumped at 980 nm **(d)**, and the same Er-RFL pumped at 1480 nm **(f)**. The values of the speckle contrast C and number of longitudinal modes m for each optical source are indicated at the side. (Adapted with permission from ref. [69].)

To confirm the experimental results for the Er-RFL system, we first characterized a well-known colloidal-based RL consisting of rhodamine 6G and TiO_2 nanoparticles. Similarly to the work of ref. [71], the speckle-free RL emission is corroborated, and the calculated C and m values for the RL are 0.058 and 297, respectively, which is very much distinct from the respective values for the pump laser. Also, the speckle images from Figs. 3(a) and 3(b) are strikingly different, as already reported [40]. The same behavior are reproduced for the Er-RFL, in which the pump laser at 1480 nm presents m = 2 longitudinal modes, whereas the Er-RFL displays the presence of m = 204 longitudinal modes. Actually, being a multimode system is a fundamental requirement for the observation of the spin-glass type behavior in RLs, as discussed below.

On the other hand, we remark that the fluctuations of the pump source (less than 5%) were not correlated with the RFL fluctuations, as also similarly demonstrated in [42,72]. This important point is corroborated by the results displayed in Figs. 4(a) and 4(b), showing, respectively, the spectral variance of the Er-RFL system and the normalized standard deviation of both the pump laser and Er-RFL. It is thus clear from Fig. 4(b) that the pump laser fluctuations do not affect the Er-RFL fluctuations, particularly because the former was kept working all the time well above threshold, so that the kind of new physics observed around the threshold in the Er-RFL would not be detected, even if present.

Preprints (www.preprints.org) | NOT PEER-REVIEWED | Posted: 15 May 2017 doi:10.20944/preprints201705.0111.v1

Peer-reviewed version available at Appl. Sci. 2017, 7, 644; doi:10.3390/app7070644

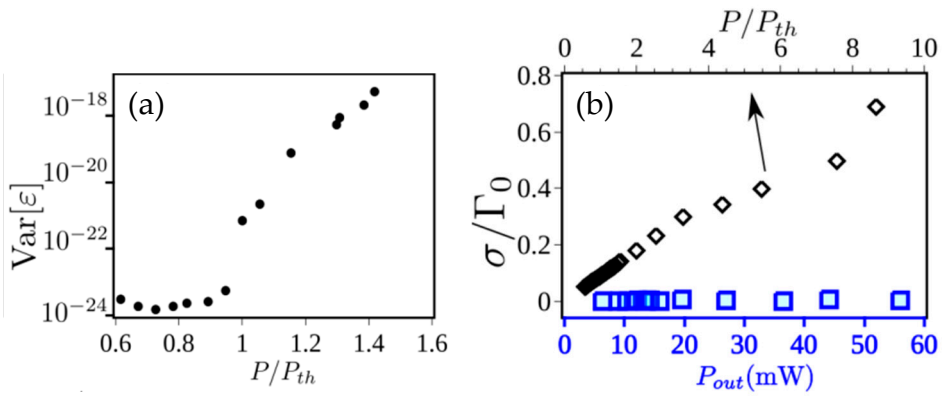

Figure 4. (a) Variance of the emitted intensity as a function of the normalized input power P/P_{th}. **(b)** Standard deviation of the maximum intensity (normalized by its average value) of the cw semiconductor pump laser (as a function of the output power P_{out}; squares) and the Er-RFL system (as a function of the normalized input power P/P_{th}; diamonds). (Reproduced with permission from ref. [68].)

3.2. Theoretical Framework

A great advance in the theoretical understanding of the combined effect of amplification, nonlinearity, and disorder in RL systems was put forward in a series of articles [73-82] published along the last decade. We start by reviewing the theoretical background [73-80] underlying the variety of photonic behaviors displayed by RLs, which relies its basis on the Langevin equations that drive the dynamics of the complex slow-amplitudes modes $a_k(t)$,

$$\frac{da_k}{dt} = -\frac{\partial H}{\partial a_k^*} + F_k, \tag{1}$$

where F_k is a Gaussian (white) uncorrelated noise term and the general complex-valued functional H reads (following closely the notation of [78])

$$H = \sum_{\{k_1k_2\}'} g^{(2)}_{k_1k_2}\, a_{k_1}a^*_{k_2} + \frac{1}{2}\sum_{\{k_1k_2k_3k_4\}'} g^{(4)}_{k_1k_2k_3k_4}\, a_{k_1}a^*_{k_2}a_{k_3}a^*_{k_4}. \tag{2}$$

The symbol $\{...\}'$ implies the frequency-matching conditions $|\omega_{k_1} - \omega_{k_2}| < \gamma$ and $|\omega_{k_1} - \omega_{k_2} + \omega_{k_3} - \omega_{k_4}| < \gamma$ in the quadratic and quartic terms, respectively, with γ denoting the finite linewidth of the modes. The physical origin of the quadratic coupling $g^{(2)}_{k_1k_2}$ lies in the spatially inhomogeneous refractive index, as well as in the nonuniform distribution of the gain and effective damping contribution due to the cavity leakage. In systems with null or weak leakage in which the off-diagonal contribution is negligible, the real part of the diagonal coupling accounts for the coefficient rates of amplification (γ_k) and radiation loss (α_k) through $g^{(2)R}_{kk} = Re\{g^{(2)}_{kk}\} = \alpha_k - \gamma_k$. On the other hand, the quartic coupling $g^{(4)}_{k_1k_2k_3k_4}$ is related to the modulation of the nonlinear $\chi^{(3)}$-susceptibility with random spatial profile [73-80].

The spatial disorder generally makes the explicit calculation of the quadratic and quartic couplings in Eq. (2) rather difficult. In fact, in [73-80] these couplings have been considered as quenched Gaussian variables, with probability distributions independent of the mode combinations $\{k_1k_2\}'$ and $\{k_1k_2k_3k_4\}'$, respectively. In a mean-field approach [73-80], all modes are coupled and the frequency-matching restrictions are relaxed. In addition, by considering the total optical intensity, $I = \sum_k c_k|a_k|^2$, as a constant, with time-independent prefactors c_k, the real part H^R of the functional (2) becomes analogue to the Hamiltonian of the p-spin model with spherical constraint [78,80,83], which is given by a sum of quadratic (p = 2) and quartic (p = 4) terms with

Preprints (www.preprints.org) | NOT PEER-REVIEWED | Posted: 15 May 2017 doi:10.20944/preprints201705.0111.v1

Peer-reviewed version available at Appl. Sci. 2017, 7, 644; doi:10.3390/app7070644

Gaussian-distributed couplings. It is important to note that in the photonic-to-magnetic analogy the excitation (pump) energy plays the role of the inverse temperature and the amplitudes of the modes correspond to the spins variables.

An equilibrium statistical physics approach, with the replica trick applied to H^R, led to a phase diagram for the pumping rate as a function of the disorder strength [78,79]. Photonic paramagnetic, ferromagnetic, phase-locking-wave, and replica-symmetry-breaking (RSB) spin-glass phases have been characterized [78,79], depending on the trend of the disorder to hamper the synchronous oscillation of the modes. For example, at low input powers the modes oscillate incoherently in an uncorrelated way. This phase is analogue to the paramagnetic behavior in spins systems at high temperatures. On the other hand, in the RL regime above the threshold the modes acquire phase coherence and nontrivial correlations (see below), similarly to the spin-glass phase at low temperatures in disordered magnets. Moreover, as also reported for spin-glass systems [84], the RL regime presents the property of RSB [73-80].

In the magnetic context, the concept of RSB was introduced [84] to justify that identical spin-glass systems with the same distribution of spins interactions and under identical conditions (i.e., *replicas* of the spin system) can reach different states and lead to distinct measurements of observables. The characterization of RSB in spins systems is performed through the analysis of the distribution of values of a spin-spin correlation function (a replica overlap parameter) [84]. Essentially, if the distribution of such values is centered around zero, the replicas are considered symmetric, a scenario observed in the paramagnetic phase. However, if such distribution peaks at non-zero values of the replica overlap parameter then the symmetry of replicas is broken, and a RSB spin-glass phase can thus emerge. On the other hand, in the photonic context an analogue correlation function between modes can be also suitably defined [42,79] (see below), whose distribution of values determine in a similar way the presence or not of photonic RSB properties.

On the experimental side, the very first evidence of photonic RSB glassy behavior in a RL system arose in the 2D functionalized T_5OC_x oligomer amorphous solid-state material [42]. Subsequent demonstrations appeared in 3D functionalized TiO_2 particle-based dye-colloidal [85] and neodymium-doped YBO_3 solid-state [82] RLs. Here we highlight that the RSB glassy phase has been also characterized in the above-mentioned Er-RFL system [68,69]. The emergence of such phase is actually justified since the Er-RFL presents the disorder and nonlinear ingredients necessary to the theoretical description through an effective photonic Hamiltonian with the general features discussed above.

We now turn to the discussion on the statistical regimes of intensity fluctuations in RL systems. Noteworthy, the set of Langevin equations, given by Eq. (1), also provides the underlying theoretical basis for such analysis. Indeed, by writing $I_k = c_k|a_k|^2$, manipulation of Eq. (1) yields [82]

$$\frac{1}{c_{k_2}}\frac{dI_{k_2}}{dt} = -2Re\left\{\sum_{\{k_1\}'} g^{(2)}_{k_1k_2}\, a_{k_1}a^*_{k_2} + \frac{1}{2}\sum_{\{k_1k_3k_4\}'}\left[g^{(4)}_{k_1k_2k_3k_4} + g^{(4)}_{k_1k_4k_3k_2}\right] a_{k_1}a^*_{k_2}a_{k_3}a^*_{k_4} + a^*_{k_2}F_{k_2}\right\}. \quad (3)$$

The restricted sum in the quartic coupling generally involves three classes of mode combinations [73,86]: $\omega_{k_1} = \omega_{k_2}$ and $\omega_{k_3} = \omega_{k_4}$, $\omega_{k_1} = \omega_{k_4}$ and $\omega_{k_2} = \omega_{k_3}$, and the remaining possibilities satisfying the frequency-matching conditions, which have been usually disregarded [73,86]. We consider the diagonal contribution in the quadratic coupling to dominate over the off-diagonal part. By expressing the optical noise as the sum of additive and multiplicative statistically independent

Preprints (www.preprints.org) | NOT PEER-REVIEWED | Posted: 15 May 2017 doi:10.20944/preprints201705.0111.v1

Peer-reviewed version available at Appl. Sci. 2017, 7, 644; doi:10.3390/app7070644

stochastic processes [87], so that $F_k(t) = F_k^{(0)}(t) + a_k(t)F_k^{(1)}(t)$, and considering slow-amplitude modes $a_k(t)$ (if compared to the rapidly evolving phase dynamics), we obtain the Fokker-Planck equation [81,82,87] for the probability density function (PDF) of emission intensity,

$$\frac{\partial P}{\partial t} = -\frac{\partial}{\partial I_k}[(-d_k I_k - b_k I_k^2 + 2QI_k)P] + 2Q\frac{\partial^2}{\partial I_k^2}(I_k^2 P), \quad (4)$$

where the parameter Q controls the magnitude of the multiplicative fluctuations through $\langle F_k^{(1)R}(t)F_m^{(1)R}(t')\rangle = 2Q\delta_{k,m}\delta(t-t')$, $b_k = g_{kkkk}^{(4)R}/c_k$, and

$$d_k = \sum_{n\neq k}\left[g_{kknn}^{(4)R} + g_{knnk}^{(4)R} + g_{nkkn}^{(4)R} + g_{nnkk}^{(4)R}\right] I_n/c_n - 2(\gamma_k - \alpha_k). \quad (5)$$

The steady-state solution of Eq. (4) is [81,82,87]

$$P(I_k) = A_k I_k^{-\mu_k}\exp(-b_k I_k/2Q), \quad (6)$$

with $I_k > 0$, A_k as the normalization constant, and $\mu_k = 1 + d_k/2Q$. This PDF presents a power-law decay combined with exponential attenuation. Its second moment can be very large, though still finite, depending on the value of μ_k, mainly if $b_k/2Q \ll 1$. Indeed, the experimental results obtained for the Er-RFL (see below) indicate [68] that the distribution of output intensities displays much larger variance and much stronger fluctuations close to the threshold, if compared with those below and above the threshold. In this sense, as argued below, the PDF of intensities is most properly described by the Lévy α-stable distribution [88] for a long time in cw-pumped RLs, such as the Er-RFL system [68], or during an extensive number of shots in the case of pulsed RLs [89] (Lévy-like statistical behavior).

If the values of the output intensity I fluctuate in an uncorrelated stochastic way (or even if they present finite-time correlations) and the second moment of the PDF $P(I)$ is finite, then the central limit theorem (CLT) assures that their statistical properties are driven by the Brownian (Gaussian, normal) dynamics [88]. On the other hand, if the second moment of $P(I)$ diverges, the generalized CLT states that they are governed by the Lévy statistics, which is described by the family of Lévy α-stable distributions, with Fourier transform to the k-space given by the characteristic function [88]:

$$\overline{P}(k) = \exp\{-|ck|^{\alpha}[1 - i\beta\,\mathrm{sgn}(k)\Phi] + ik\nu\}. \quad (7)$$

In Eq. (7) the Lévy index $\alpha \in (0,2]$ is the most important parameter, since it drives the type of statistics that characterizes the fluctuations of the random variables. Indeed, whereas strong fluctuations with relevant deviations from the Gaussian behavior are associated with values in the range $0 < \alpha < 2$, the Gaussian statistics with weak fluctuations and the result of the CLT are recovered for the boundary value $\alpha = 2$. The other parameters describe the asymmetry or skewness ($\beta \in [-1,1]$), location ($\nu \in (-\infty,\infty)$), scale ($c \in (0, \infty)$), and $\Phi = \tan(\pi\alpha/2)$ if $\alpha \neq 1$, whereas $\Phi = -(2/k)\ln|k|$ if $\alpha = 1$. Though the Lévy PDF displays closed analytical form only for a few values of α (e.g., the Cauchy distribution arises for $\alpha = 1$ and $\beta = 0$), its large-I asymptotic behavior is power-law tailed, $P(I) \sim I^{-\mu}$, with exponent $\mu = 1 + \alpha$. Conversely, it is also true that random variables with power-law distribution are governed by the Lévy PDF with $\alpha = \mu - 1$ if $1 < \mu < 3$ (diverging second moment), and by the $\alpha = 2$ Gaussian statistics if $\mu \geq 3$ (finite second moment) [88]. Therefore, Eq. (7) can suitably describe both Gaussian and Lévy statistical regimes, depending only on the value of the single parameter α.

In the present case of intensity fluctuations, as well as in any case of realistic stochastic phenomena, a PDF with diverging second moment actually represents an unphysical possibility. Nevertheless, it has been demonstrated [90] that a truncated power-law PDF with large but finite

Preprints (www.preprints.org) | NOT PEER-REVIEWED | Posted: 15 May 2017 doi:10.20944/preprints201705.0111.v1

Peer-reviewed version available at Appl. Sci. 2017, 7, 644; doi:10.3390/app7070644

second moment behaves rather similarly to the Lévy PDF to a considerable extent, defining the so-called Lévy-like behavior, with the crossover to the Brownian dynamics predicted by the CLT attained only in a very long term [90,91]. In this sense, truncation schemes can be suitably implemented, for instance, by restricting the values of the random variable to a finite range [90,91], with $P(I) = 0$ for $I > I_{max}$, or by tempering the power law with an exponential attenuation [81,82,89], $P(I) \sim I^{-\mu}\exp(-\eta I)$, similarly to Eq. (6).

In addition to the description above of the truncated power-law with exponential attenuation, based on the Langevin dynamics of the amplitudes of the normal modes, the power-law PDF $P(I) \sim I^{-\mu}$ has been also theoretically justified in which $\mu = 1 + \ell_g/\langle l \rangle$, with ℓ_g and $\langle l \rangle$ denoting, respectively, the gain length of the active medium and the average length of the photon trajectories within the sample [92].

3.2. Lévy Statistics and Glassy Behavior in Er-RFL

We now turn to the statistical analysis of the intensity spectra. Figures 5(a)-(c) display 5000 spectra for each input power, from which the intensity fluctuations can be appreciated in the regimes below [Fig. 5(a)], around [Fig. 5(b)], and above [Fig. 5(c)] the threshold [68]. According to the previous discussion, the strong intensity fluctuations observed near the threshold suggest that the PDF of the output intensities can be described by the family of Lévy α-stable distributions, including the Lévy statistical regime if $0 < \alpha < 2$ and the Gaussian limit if $\alpha = 2$. Figures 5(d)-(f) portrait the distributions $P(I)$ obtained from the data of Figs. 5(a)-(c), as well as the respective best fits to Eq. (7) by applying the quantile-based method [93,94]. Best-fit values of the parameters are summarized in Table 1. The values of α are consistent with the Gaussian profiles ($\alpha = 2.0$) shown in Figs. 5(d) and 5(f) respectively below and above the threshold, and also with the Lévy-like PDF ($\alpha = 1.3$) around the threshold, observed in Fig. 5(e). The unit value of β indicating maximum skewness of the distribution in all cases reflects the asymmetry related to the positiveness of the intensity. Also, the values of the location parameter ν in the Gaussian regimes, $\nu = 0.858$ for $P/P_{th} = 0.6$ and $\nu = 0.682$ for $P/P_{th} = 1.8$, agree with the mean values respectively observed in Figs. 5(d) and 5(f). Indeed, the actual Gaussian distributions which are equivalent to the $\alpha = 2$ Lévy PDFs in Figs. 5(d) and 5(f) present mean ν and standard deviation $\sqrt{2}c$, as theoretically predicted [88]. Interestingly, when comparing the Gaussian regimes below and above the threshold, we notice a considerable broadening of the PDF $P(I)$ at $P/P_{th} = 1.8$, leading to a wider spread of intensities [Fig. 5(f)]. This result is associated with the larger second moment of the distribution and more intense fluctuations observed above the threshold. Those fluctuations remain, however, still much weaker than the ones measured in the crossover region.

Preprints (www.preprints.org) | NOT PEER-REVIEWED | Posted: 15 May 2017 doi:10.20944/preprints201705.0111.v1

Peer-reviewed version available at Appl. Sci. 2017, 7, 644; doi:10.3390/app7070644

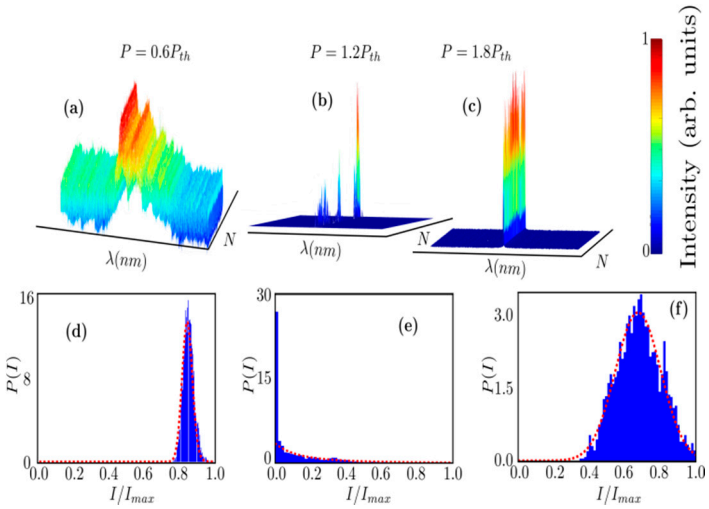

Figure 5. (a)-(c) 5000 intensity spectra of the Er-RFL system for each input power **(a)** below, **(b)** around, and **(c)** above the threshold. **(d)-(f)** PDFs $P(I)$ of maximum intensities obtained from the data shown in **(a)-(c)**. The best fits using Eq. (7) are depicted in dotted lines and portrait Gaussian profiles **(d)** below and **(f)** above the threshold ($\alpha = 2.0$), and **(e)** a Lévy distribution ($\alpha = 1.3$) around the threshold. (Reproduced with permission from ref. [68].)

The main result confirming the Lévy behavior of output intensities of the Er-RFL system is shown in Fig. 6. With basis on ref. [68], we first notice that the variation of the Lévy index α as a function of the normalized input power clearly points to the presence of three distinct statistical regimes. Indeed, as P/P_{th} increases the statistics of output intensities progressively shifts from the prelasing Gaussian ($\alpha = 2$) to the Lévy ($0 < \alpha < 2$) behavior around the threshold, and to the subsequent Gaussian ($\alpha = 2$) regime deep in the RL phase. Noticeably, this sequence also resembles the statistical behavior of the output intensity of 3D bulk RLs [82,89,93,95,96]. The independence on dimensionality of the Lévy character of intensity fluctuations finds support in the theoretical analysis based on Langevin equations, which is considered to hold irrespective of the spatial dimension [69,82].

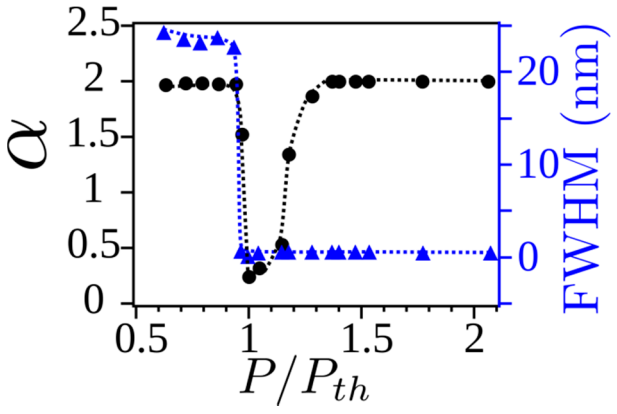

Figure 6. Lévy index α (circles) and FWHM (triangles) as a function of the normalized pump power. Three statistical regimes of intensity fluctuations are observed: prelasing Gaussian ($\alpha = 2$), Lévy-like RL ($0 < \alpha < 2$) around the threshold, and Gaussian RL ($\alpha = 2$) well above threshold. The sharp decrease in α at the first Gaussian-to-Lévy transition nicely coincides with the abrupt change in FWHM at the RL threshold. (Reproduced with permission from ref. [68].)

Preprints (www.preprints.org) | NOT PEER-REVIEWED | Posted: 15 May 2017 doi:10.20944/preprints201705.0111.v1

Peer-reviewed version available at Appl. Sci. 2017, 7, 644; doi:10.3390/app7070644

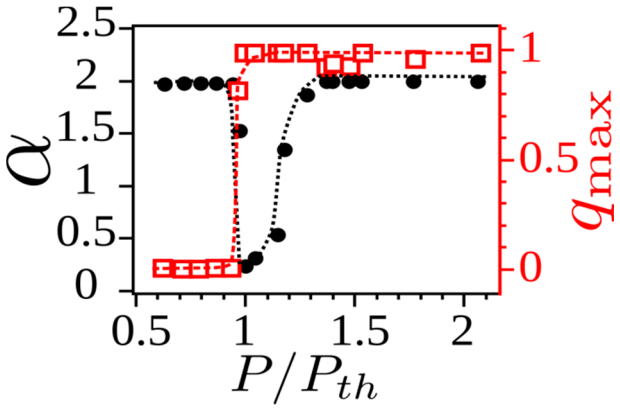

Figure 7. Lévy index α (circles) and parameter $|q| = q_{max}$ at which the PDF P(q) of replica overlaps of intensity fluctuations is maximum (squares) as a function of the normalized input power. The abrupt decrease in α at the first Gaussian-to-Lévy transition nicely coincides with the photonic transition from the $q_{max} \cong 0$ replica-symmetric paramagnetic prelasing behavior to the $q_{max} \cong 1$ RSB spin-glass RL phase of the Er-RFL system. Dotted lines are guide to the eyes. (Reproduced with permission from ref. [68].)

We also notice in Fig. 6 that the abrupt decrease in α at the onset of RL behavior is closely related to the sharp linewidth reduction observed in Fig. 2. Therefore, our results for the Er-RFL system corroborate the suggestion of [93] that the transition from the Gaussian to the Lévy regime in RLs could be used as a universal identifier of the RL threshold. In fact, we also included in Fig. 6 the FWHM measurement, whose drastic change at the threshold nicely coincides with the first Gaussian-to-Lévy transition. For higher input powers, after reaching a minimum around the threshold the index α smoothly raises back to the Gaussian value $\alpha = 2$ achieved above threshold.

Table 1. Summary of best fit parameters to Eq. (7) for the intensity distributions of Figs. 5(d)-(f) [68].

Input power	α	β	c	ν
$P/P_{th} = 0.6$	1.9	1.0	0.021	0.858
$P/P_{th} = 1.2$	1.3	1.0	0.061	-0.193
$P/P_{th} = 1.8$	2.0	1.0	0.091	0.682

We finally discuss the connection of the above findings with the photonic spin-glass behavior recently reported in the Er-RFL system [68,69].

As mentioned, the characterization of the photonic RSB glassy phase in the RL regime requires the calculation of mode-mode correlations, either among amplitudes, phases or intensity fluctuations. In the latter case, which can be accessed experimentally, the overlap parameter is defined as [42,79]

$$q_{\gamma\beta} = \frac{\sum_k \Delta_\gamma(k)\Delta_\beta(k)}{\sqrt{\left[\sum_k \Delta_\gamma^2(k)\right]\left[\sum_k \Delta_\beta^2(k)\right]}}, \quad (8)$$

where $\gamma, \beta = 1,2,\ldots,N_s$ denote the replica labels ($N_s = 5000$ in ref. [68]), the average intensity at the wavelength indexed by k reads $\langle I\rangle(k) = \sum_{\gamma=1}^{N_s} I_\gamma(k)/N_s$, and the intensity fluctuation is $\Delta_\gamma(k) = I_\gamma(k) - \langle I\rangle(k)$. In the present context, each output spectrum is considered a replica, i.e., a copy of the Er-RFL system under fairly identical experimental conditions. The PDF P(q), analogue to the Parisi

Preprints (www.preprints.org) | NOT PEER-REVIEWED | Posted: 15 May 2017 doi:10.20944/preprints201705.0111.v1

Peer-reviewed version available at Appl. Sci. 2017, 7, 644; doi:10.3390/app7070644

order parameter in the RSB spin-glass theory of disordered magnetic systems [84], describes the distribution of values $q = q_{\gamma\beta}$ of the mode-mode correlations between intensity fluctuations (replica overlaps), signaling a replica-symmetric paramagnetic or a RSB spin-glass phase if its maximum occurs exclusively at $q_{max} = 0$ (no RSB) or also at values $|q_{max}| \neq 0$ (RSB), respectively.

Figure 7 shows a remarkable agreement between the onset of the Lévy statistical regime of intensity fluctuations and the emergence of the RSB glassy RL phase in Er-RFL. Indeed, we observe that both Lévy and spin-glass behaviors are simultaneously present around the threshold. Therefore, besides signaling the Gaussian-to-Lévy shift in the statistics of intensity fluctuations, illustrated by Fig. 6, the RL threshold also marks the sharp phase transition from the $q_{max} \cong 0$ replica-symmetric paramagnetic prelasing regime to the $q_{max} \cong 1$ spin-glass RL phase with RSB. This coinciding behavior, firstly demonstrated in a 3D RL [82], is thus also shared by the Er-RFL system, although a recent report [97] has pointed that this might not be a universal property of RL systems. Therefore, though a complete theoretical understanding of such finding is still lacking, it is possible to trace back the common physical origin of the Lévy and glassy behaviors to the Langevin equations for the amplitudes of the normal modes, which, as discussed, are the basis to explain both the statistical regimes of intensity fluctuations and the photonic RSB spin-glass behavior of RL systems.

4. Summary and Discussion

In this work, we described the operation of a RFL based on an erbium-doped fiber imprinted with randomly-spaced Bragg gratings. By exciting the fiber with a cw diode laser, we investigated the statistical fluctuations of the output intensity emitted by the erbium ions in the near infrared. The results allowed us to identify different statistical regimes for excitation powers P below, around, and above the laser threshold, P_{th}. In particular, the Lévy statistics was clearly identified for $P \approx P_{th}$. Moreover, we also found that the probability distribution for the emitted intensity around the laser threshold reveals a glassy phase of light compatible with a RSB analogue of the spin-glass phase transition.

The studies reported here led to a deeper understanding of the physical processes underlying the RFL operation, and the results were also consistent with recent findings in 2D and 3D RLs.

As illustrated by the references cited in this paper, the research on RFLs is still a hot subject after ten years since the first demonstration. The low fabrication cost, small fiber length, and simple operation scheme enable various potential applications of RFLs, as, for example, in imaging, sensing, and optofluidics. Further research with basis on the investigation of the intensity fluctuations in RFL systems may include the study of their temporal dynamics, as well as the emergency of extreme events, analogues of rogue waves, and photonic turbulent transitions around the excitation threshold.

Acknowledgments: We thank S. J. M. Carreño, S. I. Fewo, M. Gagné, V. Jerez, R. Kashyap, B. C. Lima, L. J. Q. Maia, A. L. Moura, P. I. R. Picheira, and A. F. Silva for the fruitful collaboration. We also acknowledge the financial support from the Brazilian Agencies: Conselho Nacional de Desenvolvimento Científico e Tecnológico (CNPq) and Fundação de Amparo à Ciência e Tecnologia do Estado de Pernambuco (FACEPE). The work was performed in the framework of the National Institute of Photonics (INCT de Fotônica) and PRONEX-CNPq/FACEPE projects.

Author Contributions: C.B.A., A.S.L.G. and E.P.R. contributed equally to this review.

Conflicts of Interest: The authors declare no conflict of interest.

Preprints (www.preprints.org) | NOT PEER-REVIEWED | Posted: 15 May 2017 doi:10.20944/preprints201705.0111.v1

Peer-reviewed version available at Appl. Sci. 2017, 7, 644; doi:10.3390/app7070644

References

1. Ambartsumyan, R.V.; Basov, N.G.; Kryukov, P.G.; Letokhov, V.S. Laser with nonresonant feedback. *JETP Lett.* **1966**, *3*, 167-169.
2. Letokhov, V.S. Generation of light by a scattering medium with negative resonance absorption. *Sov. Phys. JETP* **1968**, *26*, 835-840.
3. Ambartsumyan, R.V.; Kryukov, P.G.; Letokhov, V.S. Dynamics of emission line narrowing for a laser with nonresonant feedback. *Sov. Phys. JETP* **1967**, *24*, 1129-1134.
4. Ambartsumyan, R.V.; Basov, N.G.; Letokhov, V.S. Frequency stability of a HeNe laser with nonresonant feedback. *IEEE Trans. Instrum. Measure.* **1968**, *IM-17*, 338-343.
5. Ambartsumyan, R.V.; Kryukov, P.G.; Letokhov, V.S.; Matveets, Y.A. Emission statistics of a laser with nonresonant feedback. *JETP Lett.* **1967**, *5*, 312-314.
6. Letokhov, V.S. Stimulated radio emission of the interstellar medium. *JETP Lett.* **1966**, *4*, 321-323.
7. Lavrinovich, N.N.; Letokhov, V.S. The possibility of laser effect in stellar atmospheres. *Sov. Phys. JETP* **1975**, *40*, 800-805.
8. Letokhov, V.S. Astrophysical lasers. *Quantum Electron.* **2002**, *32*, 1065-1079.
9. Johansson, S.; Letokhov, V.S. Astrophysical lasers operating in optical Fe II lines in stellar ejecta of Eta Carinae. *Astron. & Astrophys.* **2004**, *428*, 427-509.
10. Noginov, M.A. *Solid State Random Lasers*, Springer Series in Optical Sciences; Springer: New York, U.S.A., 2005.
11. Lawandy, N.M.; Balachandran, R.M.; Gomes, A.S.L.; Sauvian, E. Laser action in strongly scattering medium. *Nature*, **1994**, *368*, 436-438.
12. Ye, L.; Zhao, C.; Feng, Y.; Gu, B.; Cui, Y.; Lu, Y. Study on the polarization of random lasers from dye-doped nematic liquid crystals. *Nanoscale Res. Lett.* **2017**, *12*, 27.
13. Abegão, L.M.G.; Manoel, D.S.; Otuka, A.J.G.; Ferreira, P.H.D.; Vollet, D.R.; Donatti, D.A.; De Boni, L.; Mendonça, C.R.; de Vicente, F.S.; Rodrigues Jr., J.J.; Alencar, M.A.R.C. Random laser emission from a rhodamine B-doped GPTS/TEOS-derived organic/sílica monolithic xerogel. *Laser Phys. Lett.* **2017**, *14*, 065801.
14. Shasti, M.; Coutino, P.; Mukherjee, S.; Varanytsia, A.; Smith, T.; Luchette, A.P.; Sukhomlinova, L.; Kosa, T.; Munoz, A.; Taheri, B. Reverse mode switching of the random laser emission in dye doped liquid crystals under homogeneous and inhomogeneous electric fields. *Photon. Res.* **2016,** *4*, 7-12.
15. Anderson, B.R.; Gunawidjaja, R.; Eilers, H. Self-healing organic-dye-based random lasers. *Opt. Lett.* **2015**, *40*, 577-580.
16. Gomes, A.S.L.; Carvalho, M.T.; Dominguez, C.T.; de Araújo, C.B.; Prasad, P.N. Direct three-photon excitation of upconversion random laser emission in a weakly scattering organic colloidal system. *Opt. Express* **2014**, *22*, 14305-14310.
17. Knitter, S.; Kues, M.; Fallnich, C.; Emission polarization of random lasers in organic dye solutions. *Opt. Lett.* **2012**, *37*, 3621-3623.
18. Chen, Y.; Herrnsdorf, J.; Guilhabert, B.; Zhang, Y.; Watson, I.M.; Gu, E.; Laurand, N.; Dawson, M.D. Colloidal quantum dot random laser. *Opt. Express* **2011**, *19*, 2996-3003.
19. Dominguez, C.T.; Gomes, M.A.; Macedo, Z.S.; de Araújo, C.B.; Gomes, A.S.L. Multi-photon excited coherent random laser emission in ZnO powders. *Nanoscale* **2015**, *7*, 317-323.
20. Moura, A.L.; Jerez, V.; Maia, L.J.Q.; Gomes, A.S.L.; de Araújo, C.B. Multi-wavelength emission through self-induced second-order wave-mixing processes from a Nd^{3+} doped crystalline powder random laser. *Sci. Rep.* **2015**, *5*, 13816.
21. Moura, A.L.; Carreño, S.J.M.; Pincheira, P.I.R.; Fabris, Z.V.; Maia, L.J.Q.; Gomes, A.S.L.; de Araújo, C.B. Tunable ultraviolet and blue light generation from Nd:YAB random laser bolstered by second-order nonlinear processes. *Sci. Rep.* **2016**, *6*, 27107.
22. Polson, R.C.; Chipouline, A.; Vardeny, Z.V. Random lasing in π-conjugated films and infiltrated opals. *Adv. Mater.* **2001**, *13*, 760–764.
23. Meng, X.; Fujita, K.; Murai, S.; Tanaka, K. Coherent random lasers in weakly scattering polymer films containing silver nanoparticles. *Phys. Rev. A* **2009**, *79*, 053817.
24. Costela, A.; Garcia-Moreno, I.; Cerdan, L.; Martin, V.; Garcia, O.; Sastre, R. Dye-doped POSS solutions: random nanomaterials for laser emission. *Adv. Mater.* **2009**, *21*, 4163–4166.

Preprints (www.preprints.org) | NOT PEER-REVIEWED | Posted: 15 May 2017 doi:10.20944/preprints201705.0111.v1

Peer-reviewed version available at Appl. Sci. 2017, 7, 644; doi:10.3390/app7070644

25. Tulek, A.; Polson, R.C.; Vardeny, Z.V. Naturally occurring resonators in random lasing of π-conjugated polymer films. *Nat. Phys.* **2010**, *6*, 303–310.
26. Polson, R.C.; Raikh, M.E.; Vardeny, Z.V. Random lasing from weakly scattering media; spectrum universality in DOO–PPV polymer films. Physica E **2002**, *13*, 1240–1242.
27. Dos Santos, M.V.; Dominguez, C.T.; Schiavon, J.V.; Barud, H.S.; de Melo, L.S.A.; Ribeiro, S.J.L.; Gomes, A.S.L.; de Araújo, C.B. Random laser action from flexible biocellulose-based device. *J. Appl. Phys.* **2014**, *115*, 083108.
28. Yu, S.F.; Yuen, C.; Lau, S.P.; Park, W.I.; Yi, G.-C. Random laser action in ZnO nanorod arrays embedded in ZnO epilayers. *Appl. Phys. Lett.* **2004**, *84*, 3241-3243.
29. Wang, Z.; Shi, X.; Wei, S.; Sun, Y.; Wang, Y.; Zhou, J.; Shi, J.; Liu, D. Two-threshold silver nanowire-based random laser with different dye concentrations. *Laser Phys. Lett.* **2014**, *11*, 095002.
30. Gao, F; Morshed, M.M.; Bashar, S.B.; Zheng, Y.; Shi, Y.; Liu, J. Electrically pumped random lasing based on an Au–ZnO nanowire Schottky junction. *Nanoscale* **2015**, *7*, 9505-9509.
31. Bashar, S.B.; Suja, M.; Morshed, M.; Gao, F.; Liu, J. An Sb-doped p-type ZnO nanowire based random laser diode. *Nanotech.* **2016**, *27*, 065204.
32. Baudouin, Q.; Mercadier, N.; Guarrera, V.; Guerin, W.; Kaiser, R. A cold-atom random laser. *Nat. Phys.* **2013**, *9*, 357-360.
33. Van der Molen, K.L.; Mosk, A.P.; Lagendijk, A.D. Intrinsic intensity fluctuations in random lasers. *Phys. Rev. A* **2006**, *74*, 053808.
34. Van der Molen, K.L.; Tjerkstra, R.W.; Mosk, A.P.; Lagendijk, A.D. Spatial extent of random laser modes. *Phys. Rev. Lett.* **2007**, *98*, 143901.
35. Wiersma, D.S. The physics and applications of random lasers. *Nat. Phys.* **2008**, *4*, 359-367.
36. Leonetti, M.; Conti, C.; Lopez, C. The mode-locking transition of random lasers. *Nat. Photon.* **2011**, *5*, 615-617.
37. Ignesti, E.; Tommasi, F.; Fini, L.; Martelli, F.; Azzali, N.; Cavalieri, S. A new class of optical sensors: a random laser based device. *Sci. Rep.* **2016**, *6*, 35225.
38. Bhaktha, B.N.S.; Bachelard, N.; Noblin, X.; Sebbah, P. Optofluidic random laser. *Appl. Phys. Lett.* **2012**, *101*, 151101.
39. Bachelard, N.; Gigan, S.; Noblin, X.; Sebbah, P. Adaptive pumping for spectral control of random lasers. *Nat. Phys.* **2014**, *10*, 426-431.
40. Redding, B.; Choma, M.A.; Cao, H. Speckle-free laser imaging using random laser illumination. *Nat. Photon.* **2012**, *6*, 355-359.
41. Luan, F.; Gu, B.B.; Gomes, A.S.L.; Yong, K.T.; Wen, S.C.; Prasad, P.N. Lasing in nanocomposite random media. *Nano Today* **2015**, *10*, 168-192.
42. Ghofraniha, N.; Viola, I.; Di Maria, F.; Barbarella, G.; Gigli, G.; Leuzzi, L.; Conti, C. Experimental evidence of replica symmetry breaking in random lasers. *Nat. Commum.* **2015**, *6*, 6058.
43. De Mattos, C.J.S.; Menezes, L.S.; Brito-Silva, A.M.; Gámez, M.A.M.; Gomes, A.S.L.; de Araújo, C.B.; Random fiber laser. *Phys. Rev. Lett.* **2007**, *99*, 153903.
44. Lizárraga, N.; Puente, N.P.; Chaikina, E.I.; Leskova, T.A.; Méndez, E.R. Single-mode Er-doped fiber random laser with distributed Bragg grating feedback. *Opt. Express* **2009**, *17*, 395–404.
45. Gagné, M.; Kashyap, R. Demonstration of a 3 mW threshold Er-doped random fiber laser based on a unique fiber Bragg grating. *Opt. Express* **2009**, *17*, 19067–19074.
46. Turitsyn, S.K.; Babin, S.A.; El-Taher, A.E.; Harper, P.; Churkin, D.V.; Kablukov, S.I.; Ania-Castanon, J.D.; Karalekas, V.; Podivilov, E.V. Random distributed feedback fibre laser. *Nat. Photon.* **2010**, *4*, 231–235.
47. Turitsyn, S.K.; Babin, S.A.; Churkin, D.V.; Vatnik, I.D.; Nikulin, M.; Podivilov, E.V. Random distributed feedback fibre lasers. *Phys. Rep.* **2014**, *542*, 133–193.
48. Churkin, D.V.; Sugavanam, S.; Vatnik, I.D.; Wang, Z.; Podivilov, E.V.; Babin, S.A.; Rao, Y.; Turitsyn, S.K. Recent advances in fundamentals and applications of random fiber lasers. *Adv. Opt. Photon.* **2015**, *7*, 516–569.
49. Wang, Z.; Wu, H.; Fan, M.; Zhang, L.; Rao, Y.; Zhang, W.; Jia, X. High power random fiber laser with short cavity length: theoretical and experimental investigations. *IEEE J. Sel. Top. Quant. Elect.* **2015**, *21*, 0900506.

Preprints (www.preprints.org) | NOT PEER-REVIEWED | Posted: 15 May 2017 doi:10.20944/preprints201705.0111.v1

Peer-reviewed version available at Appl. Sci. 2017, 7, 644; doi:10.3390/app7070644

50. Li, S.W.; Ma, R.; Rao, Y.J.; Zhu, Y.Y.; Wang, Z.N.; Jia, X.H.; Li, J. Random distributed feedback fiber laser based on combination of Er-doped fiber and single-mode fiber. *IEEE J. Sel. Top. Quant. Elect.* **2015**, *21*, 0900406.
51. Wu, H.; Wang, Z.; Fan, M.; Zhang, L.; Zhang, W.; Ra, Y. Role of the mirror's reflectivity in forward-pumped random fiber laser. *Opt. Express*, **2015**, *23*, 1421-1427.
52. Zhang, H.; Zhou, P.; Wang, X.; Du, X.; Xiao, H.; Xu, X. Hundred-watt-level high power random distributed feedback Raman fiber laser at 1150 nm and its application in mid-infrared laser generation. *Opt. Express* **2015**, *23*, 17138-17144.
53. Zhang, W.L.; Ma, R.; Tang, C.H.; Rao, Y.J.; Zeng, X.P.; Yang, Z.J.; Wang, Z.N.; Gong, Y.; Wang, Y.S. All optical mode controllable Er-doped random fiber laser with distributed Bragg gratings. *Opt. Lett.* **2015**, *40*, 3181-3184.
54. Wang L.; Dong, X.; Shum, P.P.; Liu, X.; Su, H. Random laser with multiphase-shifted Bragg grating in Er/Yb-codoped fiber. *J. Lightwave Technol.* **2015**, *33*, 95-99.
55. Du, X.; Zhang, H.; Wang, X.; Zhou, P.; Liu, Z. Investigation on random distributed feedback Raman fiber laser with linear polarized output. *Photon. Res.* **2015**, *3*, 28-31.
56. Tang Y.; Xu, J. A random Q-switched fiber laser. *Sci. Rep.* **2015**, *5*, 9338.
57. Yao, B.C.; Rao, Y.J.; Wang, Z.N.; Wu, Y.; Zhou, J.H.; Wu, H.; Fan, M.Q.; Cao, X.L.; Zhang, W.L.; Chen, Y.F.; Li, Y.R.; Churkin, D.; Turitsyn, S.; Wong, C.W. Graphene based widely-tunable and singly-polarized pulse generation with random fiber lasers. *Sci. Rep.* **2015**, *5*, 18526.
58. Zhang, L.; Jiang, H.; Yang, X.; Pan, W.; Feng, Y. Ultra-wide wavelength tuning of a cascaded Raman random fiber laser. *Opt. Lett.* **2016**, *41*, 215-218.
59. Du, X.; Zhang, H.; Wang, X.; Zhou, P.; Liu, Z. Short cavity-length random fiber laser with record power and ultrahigh efficiency. *Opt. Lett.* **2016**, *41*, 571-574.
60. Dontsova, E.I.; Kablukov, S.I.; Vatnik, I.D.; Babin, S.A. Frequency doubling of Raman fiber lasers with random distributed feedback. *Opt. Lett.* **2016**, *41*, 1439-1442.
61. Hu, Z.; Liang, Y.; Qian, X.; Gao, P.; Xie, K.; Jiang, H. Polarized random laser emission from an oriented disorder polymer optical fiber. *Opt. Lett*. **2016**, *41*, 2584-2587.
62. Ardakani, A.G.; Rafieipour, P. Investigation of one-dimensional Raman random lasers based on the finite-difference-time-domain method: presence of mode competition and higher-order Stokes and anti-Stokes modes. *Phys. Rev. A* **2016**, *93*, 023833.
63. Zhang, W.L.; Song, Y.B.; Zeng, X.P.; Ma, R.; Yang, Z.J.; Rao, Y.J. Temperature-controlled mode selection of Er-doped random fiber laser with disordered Bragg gratings. *Photon. Res.* **2016**, *4*, 102-105.
64. Wu, H.; Wang, Z.; Rao, Y. Tailoring the properties of cw random fiber lasers. Advanced Photonics Congress 2016 (IPR, NOMA, Sensors, Networks, SPPCom, SOF), Paper SoTu1G.3 (2016). Wu, H; Wang, Z.; Rao, Y. Tailoring the properties of cw random fiber lasers. In Advanced Photonics 2016 (IPR, NOMA, Sensors, Networks, SPPCom, SOF), OSA Technical Digest (online) (Optical Society of America, 2016); paper SoTu1G.3.
65. Babin, S.A.; Zlobina, E.A.; Kablukov, S.I.; Podivilov, E.V. High-order random Raman lasing in a PM fiber with ultimate e efficiency and narrow bandwidth. *Sci. Rep.* **2016**, *6*, 22625.
66. Zhang, W.L.; Zheng, M.Y.; Ma, R.; Gong, C.Y.; Yang, Z.J.; Peng, G.D.; Rao, Y.J. Fiber-type random laser based on a cylindrical waveguide with a disordered cladding layer. *Sci. Rep.* **2016**, *6*, 26473.
67. González, I.R.R.; Lima, B.C.; Pincheira, P.I.R.; Brum, A.A.; Macêdo, A.M.S.; Vasconcelos, G.L.; Menezes, L.S.; Raposo, E.P.; Gomes, A.S.L.; Kashyap, R. Turbulence hierarchy in a random fibre laser. *Nat. Commun.* **2017**, in press.
68. Lima, B.C.; Gomes, A.S.L.; Pincheira, P.I.R.; Moura, A.L.; Gagné, M.; Raposo, E.P.; de Araújo, C.B.; Kashyap, R. Observation of Lévy statistics in one-dimensional erbium-based random fiber laser. *J. Opt. Soc. Am. B* **2017**, *34*, 293-299.
69. Gomes, A.S.L.; Lima, B.C.; Pincheira, P.I.R.; Moura, A.L.; Gagné, M.; Raposo, E.P.; de Araújo, C.B.; Kashyap, R. Glassy behavior in a one-dimensional continuous-wave erbium-doped random fiber laser. *Phys. Rev. A* **2016**, *94*, 011801(R).
70. Hokr, B.H.; Cerjan, A.; Thompson, J.V.; Yuan, L.; Liew, S.F.; Bixler, J.N.; Noojin, G.D.; Thomas, R.J.; Cao, H.; Stone, A.D.; Rockwell, B.A.; Scully, M.O.; Yakovlev, V.V. Evidence of Anderson localization effects in random Raman lasing. *SPIE Proc.* **2016**, *9731*, 973110.

Preprints (www.preprints.org) | NOT PEER-REVIEWED | Posted: 15 May 2017 doi:10.20944/preprints201705.0111.v1

Peer-reviewed version available at Appl. Sci. 2017, 7, 644; doi:10.3390/app7070644

71. Goodman, J.W. *Speckle Phenomena in Optics: Theory and Applications*; Roberts & Company: Englewood, U.S.A., 2007.
72. Zhu, G.; Gu, L.; Noginov, M.A. Experimental study of instability in a random laser with immobile scatterers. *Phys. Rev. A* **2012**, *85*, 043801.
73. Angelani, L.; Conti, C.; Ruocco, G.; Zamponi, F. Glassy behavior of light in random lasers. *Phys. Rev. B* **2006**, *74*, 104207.
74. Angelani, L.; Conti, C.; Ruocco, G.; Zamponi, F. Glassy behavior of light. *Phys. Rev. Lett.* **2006**, *96*, 065702.
75. Leuzzi, L.; Conti, C.; Folli, V.; Angelani, L.; Ruocco, G. Phase diagram and complexity of mode-locked lasers: from order to disorder. *Phys. Rev. Lett.* **2009**, *102*, 083901.
76. Conti, C.; Leuzzi, L. Complexity of waves in nonlinear disordered media. *Phys. Rev. B* **2011**, *83*, 134204.
77. Antenucci, F.; Conti, C.; Crisanti, A.; Leuzzi, L. General phase diagram of multimodal ordered and disordered lasers in closed and open cavities. *Phys. Rev. Lett.* **2015**, *114*, 043901.
78. Antenucci, F.; Crisanti, A.; Leuzzi, L. Complex spherical 2+4 spin glass: a model for nonlinear optics in random media. *Phys. Rev. A* **2015**, *91*, 053816.
79. Antenucci, F.; Crisanti, A.; Leuzzi, L. The glassy random laser: replica symmetry breaking in the intensity fluctuations of emission spectra. *Sci. Rep.* **2015**, *5*, 16792.
80. Antenucci, F.; Crisanti, A.; Ibáñez-Berganza, M.; Marruzzo, A.; Leuzzi, L. Statistical mechanics models for multimode lasers and random lasers. *Phil. Mag.* **2016**, *96*, 704-731.
81. Raposo, E.P.; Gomes, A.S.L. Analytical solution for the Lévy-like steady-state distribution of intensities in random lasers. *Phys. Rev. A* **2015**, *91*, 043827.
82. Gomes, A.S.L.; Raposo, E.P.; Moura, A.L.; Fewo, S.I.; Pincheira, P.I.R.; Jerez, V.; Maia, L.J.Q.; de Araújo, C.B. Observation of Lévy distribution and replica symmetry breaking in random lasers from a single set of measurements. *Sci. Rep.* **2016**, *6*, 27987.
83. Crisanti, A.; Sommers, H.-J. The spherical p-spin interaction spin glass model: the statics. *Z. Phys. B* **1992**, *87*, 341–354.
84. Mézard, M.; Parisi, G.; Virasoro, M.A. *Spin Glass Theory and Beyond*; World Scientific: Singapore, 1987.
85. Pincheira, P.I.R; Silva, A.F.; Carreño, S.J.M.; Moura, A.L.; Fewo, S.I.; Raposo, E.P.; Gomes, A.S.L.; de Araújo, C.B. Observation of photonic to paramagnetic spin-glass transition in specially-designed TiO_2 particles-based dye-colloidal random laser. *Opt. Lett.* **2016**, *41*, 3459-3462.
86. O'Bryan, I.C.L.; Sargent, I.M. Theory of multimode laser operation. *Phys. Rev. A* **1973**, *8*, 3071-3092.
87. Schenzle, A.; Brand, H. Multiplicative stochastic processes in statistical physics. *Phys. Rev. A* **1979**, *20*, 1628-1647.
88. Samorodnitsky, G.; Taqqu, M.S. *Stable Non-Gaussian Random Processes*; Chapman and Hall: London, U.K., 1994.
89. Uppu, R.; Mujumdar, S. Exponentially tempered Lévy sums in random lasers. *Phys. Rev. Lett.* **2015**, *114*, 183903.
90. Mantegna, R.N.; Stanley, H.E. Stochastic process with ultraslow convergence to a Gaussian: the truncated Lévy flight. *Phys. Rev. Lett.* **1994**, *73*, 2946-2949.
91. Bartumeus, F.; Raposo, E.P.; Viswanathan, G.M.; da Luz, M.G.E. Stochastic optimal foraging: tuning intensive and extensive dynamics in random searches. *PLoS ONE* **2014**, *9*, e106373.
92. Lepri, S.; Cavalieri, S.; Oppo, G.-L.; Wiersma, D.S. Statistical regimes of random laser fluctuations. *Phys. Rev. A* **2007**, *75*, 063820.
93. Uppu, R.; Mujumdar, S. Lévy exponents as universal identifiers of threshold and criticality in random lasers. *Phys. Rev. A* **2014**, *90*, 025801.
94. McCulloch, J.H. Simple consistent estimators of stable distribution parameters. *Commun. Stat. Simul.* **1986**, *15*, 1109-1136.
95. Uppu, R.; Tiwari, A.K.; Mujumdar, S. Identification of statistical regimes and crossovers in coherent random laser emission. *Opt. Lett.* **2012**, *37*, 662-664.
96. Uppu, R.; Mujumdar, S. Dependence of the Gaussian-Lévy transition on the disorder strength in random lasers. *Phys. Rev. A* **2013**, *87*, 013822.
97. Tommasi, F.; Ignesti, E.; Lepri, S.; Cavalieri, S. Robustness of replica symmetry breaking phenomenology in random laser. *Sci. Rep.* **2016**, *6*, 37113.